# Effects of plasma shaping on nonlinear gyrokinetic turbulence

E. A. Belli,[1,a)] G. W. Hammett,[1] and W. Dorland[2]
[1]*Princeton Plasma Physics Laboratory, Princeton, New Jersey 08543, USA*
[2]*Department of Physics, University of Maryland, College Park, Maryland 20742, USA*

The effects of flux surface shape on the gyrokinetic stability and transport of tokamak plasmas are studied using the GS2 code [M. Kotschenreuther, G. Rewoldt, and W. M. Tang, Comput. Phys. Commun. **88**, 128 (1995); W. Dorland, F. Jenko, M. Kotschenreuther, and B. N. Rogers, Phys. Rev. Lett. **85**, 5579 (2000)]. Studies of the scaling of nonlinear turbulence with shaping parameters are performed using analytic equilibria based on interpolations of representative shapes of the Joint European Torus [P. H. Rebut and B. E. Keen, Fusion Technol. **11**, 13 (1987)]. High shaping is found to be a stabilizing influence on both the linear ion-temperature-gradient (ITG) instability and the nonlinear ITG turbulence. For the parameter regime studied here, a scaling of the heat flux with elongation of $\chi \sim \kappa^{-1.5}$ or $\kappa^{-2.0}$, depending on the triangularity, is observed at fixed average temperature gradient. While this is not as strong as empirical elongation scalings, it is also found that high shaping results in a larger Dimits upshift of the nonlinear critical temperature gradient due to an enhancement of the Rosenbluth-Hinton residual zonal flows. © *2008 American Institute of Physics*. [DOI: 10.1063/1.2972160]

## I. INTRODUCTION

Experimental studies indicate that plasma shaping effects are important in improving the performance of tokamaks. Multi-tokamak studies of macroscopic stability and global confinement have shown that increased shaping (elongation and triangularity) generally leads to significant increases in the energy confinement time $\tau_E$,[1,2] in the $\beta$ stability limit,[3] and in the Greenwald density limit.[4] Observations of the favorable effects of shaping in individual tokamaks include, for example, significant increases in the $\beta$ stability limit with increased elongation and triangularity in DIII-D,[5,6] simultaneous high confinement and high density relative to the Greenwald density limit with increased triangularity in high-mode (H-mode) discharges with edge localized modes (ELMs) in the Joint European Torus (JET),[7] and increased electron confinement time with increased elongation in low-mode (L-mode) electron cyclotron-heated discharges, with additional enhancements at low-to-negative triangularities, in the Tokamak à Configuration Variable (TCV) experiment.[8] These effects are generally attributable to an allowance for higher plasma current at fixed $q$, which is generally constrained by the kink instability.

The effects of shaping on plasma microturbulence and transport are, however, not fully understood. In this paper, these effects are studied using high resolution, fully electromagnetic, five-dimensional gyrokinetic simulations. In relation to gyrokinetic stability, shaping the plasma can influence the ion-temperature-gradient (ITG) turbulence by changing the local magnetic shear.[9,10] Specifically, the toroidal ITG instability is driven by bad-curvature effects. However, because particles that produce an eddy tend to follow the field lines, ITG turbulence can be reduced by reversed magnetic

shear, which twists an eddy in a short distance to point in the good-curvature direction. In contrast, for positive magnetic shear, convective cells tend to remain oriented in the $\nabla R$ direction and are thus more strongly driven. (An illustration of this can be found in Fig. 2 of Ref. 10.) Locally reversed magnetic shear is most commonly produced naturally by squeezing the field lines at high pressure, creating the so-called "second stability" regime, which was first predicted by ideal magnetohydrodynamic (MHD) theory[11] and provides the basis behind the design of advanced tokamak[12] and spherical torus[13] configurations. However, locally reversed magnetic shear can also be produced by changing the plasma shape, such as varying the elongation and triangularity, since this changes the poloidal magnetic field. These effects are explored here.

While the effects of shaping have been studied theoretically in some detail with respect to gyrokinetic linear stability,[14–16] the effects of shaping on nonlinear gyrokinetic microturbulence are not well known. Although some gyrokinetic studies of nonlinear turbulent transport in noncircular geometry have been done recently,[17–19] most systematic studies of shaping effects have been performed with gyrofluid simulations. Most notably, shaping studies by Waltz and Miller[16] using a coupling of the analytic Miller local equilibrium model[20] with a gyrofluid code found a general improvement with elongation at fixed zero triangularity for ITG turbulence with adiabatic electrons. More recent studies of drift Alfvén and ITG turbulence in edgelike plasmas by Kendl and Scott[21] using the gyrofluid code GEM[22,23] and numerical equilibria found a similar, though stronger, reduction of turbulent transport with increased elongation, due primarily to magnetic shear damping and additionally due to enhanced zonal shear flows for ITG turbulence parameters, but found only a weak enhancement with increased triangularity.

The goal of our studies here is to extend these previous

a)Present address: General Atomics, P.O. Box 85608, San Diego, CA 92186.
Electronic mail: bellie@fusion.gat.com.

studies to develop an understanding of and predictive models for the scaling of nonlinear turbulence levels with shaping parameters through systematic gyrokinetic simulations of plasma microturbulence in varying geometric equilibria using a realistic parametrization of elongation and triangularity and the local radial gradients of the shaping parameters. In these studies, we use the gyrokinetic code GS2,[24,25] a flux tube-based Eulerian code, which includes nonlinear effects, gyrokinetic electron dynamics, trapped particles, electromagnetic perturbations (though we focus on the electrostatic limit here), and a pitch angle scattering collision operator, coupled with the analytic Miller equilibrium model[20] to obtain realistic shaped plasma flux surfaces based on representative JET-based plasmas.

The remainder of this paper is organized as follows. In Sec. II, some general issues are discussed regarding how the simulation parameter scans were chosen, and some caveats about comparing local diffusion coefficients and global confinement time are identified. In Sec. III, the formulation of the equilibrium is described. In Sec. IV, simulation results showing the effects of shaping on gyrokinetic linear stability are presented. In Sec. V, these studies are extended to include nonlinear dynamics, and scalings of the nonlinear ITG turbulence with shaping, including comparisons with empirical scaling laws, are shown. The effects of shaping on the Dimits nonlinear shift of the critical temperature gradient are also presented and further described via analysis of the Rosenbluth-Hinton component of the zonal flows. Finally, a brief summary of the results is given in Sec. VI.

## II. METHODOLOGY AND PARAMETER SCAN CHOICES

Before going on, we first discuss some general issues about how the shaping scans are done in this paper and their physical motivation. There are various possible choices that could be made of which parameters to hold fixed while doing these scans, and there is not necessarily a best set of choices for all purposes. One issue is that there are many shaping parameters (nine local geometric parameters, plus other profile parameters), and we have chosen a few particular slices through this multidimensional space to make the problem manageable. The approach we adopted for this work, which is described in detail in Sec. III, basically provides interpolations from the circular limit to a standard JET shape and extrapolations beyond that to stronger shaping.

A main issue is the interpretation of the simulation transport results in relation to empirical global confinement scalings. Empirical scalings of the global confinement time $\tau_E$ are usually expressed in terms of engineering variables, like the total plasma current $I_p$ and heating power $P$, while turbulence theories for local fluxes are expressed in terms of local parameters, such as the magnetic field $B$ and plasma temperature, and geometric quantities related to the structure of the magnetic field, such as the inverse winding number $q$ (and thus the connection length $\sim Rq$ between the good- and bad-curvature regions of the plasma), the flux-surface averaged magnetic shear $\hat{s}$, the elongation and triangularity of flux surfaces and their gradients (which affect the local magnetic shear that varies within a flux surface), etc. Most of the

favorable shaping dependence observed in experiments is well captured implicitly through the dependence on the current, i.e., $\tau_E \propto I_p$, basically because a highly elongated and triangular plasma can carry a lot more current at fixed $q$ since $I_p \propto a^2 B_T f_s(\kappa, \delta)/q_{95}$, where $a$ is the midplane minor radius, $B_T$ is the toroidal magnetic field, and an expression for the dependence of $f_s(\kappa, \delta)$ on edge elongation $\kappa$ and triangularity $\delta$ is given in Eq. (9). The challenge for theory then is to understand how this strong improvement with the global plasma current can be explained in terms of local physics mechanisms, including critical gradients, and thus the local or geometric parameters such as plasma shaping that more directly affect the turbulence.

While we will find some favorable dependence of the local thermal diffusivity $\chi$ on shaping parameters (at fixed temperature gradient) and some additional favorable dependence of the critical temperature gradient on shaping, these effects by themselves appear to be insufficient in fully explaining the strong shaping dependence of global confinement observed in experiments. It may be that the remaining shaping dependence enters indirectly through the edge region, via the effects of critical gradients that can lead to stiff profiles where the core results are coupled to edge boundary conditions.

This is related to the complication that there is not a simple relationship between global confinement scalings and local transport coefficients because of the strong nonlinearities and critical gradient threshold that exist in transport coefficients. (There may also be some turbulence spreading that smooths the radial dependence of $\chi$ and further complicates comparisons. This spreading is usually small in most cases, though it may become important in some cases, particularly near the edge.) For example, theoretical transport coefficients often have a basically gyro-Bohm scaling but with a critical gradient threshold,[26] e.g.,

$$\chi = \chi_0 \frac{cT}{eB} \frac{\rho_i}{R} \left( \frac{R}{L_T} - \frac{R}{L_{T,\text{crit}}} \right) H \left( \frac{R}{L_T} - \frac{R}{L_{T,\text{crit}}} \right), \qquad (1)$$

where $cT/eB$ is the Bohm factor, $\rho_i$ is the ion gyroradius, $R$ is the major radius, $1/L_T \doteq -(1/T)(dT/dr)$ is the temperature gradient scale length, $1/L_{T,\text{crit}}$ is the critical gradient scale length threshold, $H$ is a Heaviside step-function, which is zero if the temperature gradient does not exceed the critical threshold, and $\chi_0$ is a coefficient that depends on various dimensionless parameters such as $q$, $r/R$, $\kappa$, $\delta$, etc. Balancing diffusive losses with heating, i.e., $P = -n\chi dT/dr = n\chi T/L_T$, we find that the predicted temperature gradient has the form

$$\frac{R}{L_T} = \frac{R}{2L_{T,\text{crit}}} + \frac{1}{2} \sqrt{\left( \frac{R}{L_{T,\text{crit}}} \right)^2 + \frac{4P}{\chi_0 Sn(r)T^{5/2}(r)}}, \qquad (2)$$

where $S$ is a coefficient that depends on parameters such as $B$ and $R$. In many hot plasmas, the ratio $P/(\chi_0 SnT^{5/2})$ is sufficiently small that the temperature profiles are pinned to near marginal stability, i.e., $R/L_T \approx R/L_{T,\text{crit}}$, over much of the plasma radius. Only near the cooler edge would the predicted temperature gradient scale length be affected directly by the shaping dependence of the coefficient $\chi_0$. Another way to think of this is to consider the limit where the plasma is at

marginal stability everywhere. In this limit, the temperature profile is found just by integrating $dT/dr = -T/L_{T,\text{crit}}$, giving that $T(r) \approx T_{\text{ped}} \exp((a-r)/L_{T,\text{crit}})$. One would expect the dominant effect of shaping on the core temperature profile in this limit might enter through the effects that plasma shaping has on the edge/pedestal temperature $T_{\text{ped}}$ that sets the boundary condition. (We will also find in our simulation results that shaping has a favorable effect on $L_{T,\text{crit}}$.) In this case the shaping effects are rather indirect. Specifically, the effect of shaping on $\chi_0$ is most important in the edge region in determining $T_{\text{ped}}$ (or shaping may enter through ELM stability limits that set $T_{\text{ped}}$ in H-mode cases). This then sets the boundary condition for integrating the core temperature gradient at marginal stability and thus propagates this favorable shaping effect on edge turbulence or ELM limits into the core temperature profile. Some of these issues will be discussed in more detail in Sec. V A.

Because of the sensitivity of $\chi$ to small changes in the temperature gradient when near marginal stability, the best way to compare experiments and gyrokinetic codes may be in a profile-prediction mode, where the gyrokinetic code is feedback controlled to predict the temperature gradient that would give the experimental heating power, instead of the usual approach of a $\chi$-prediction mode, where the gyrokinetic code predicts the turbulent $\chi$ given an experimentally measured temperature gradient. There is recent interest in developing such a profile-prediction capability with gyrokinetic codes, including fully self-consistent coupling with transport codes. However, in this paper, for simplicity, we will study the effects of shaping on gyrokinetic predictions of $\chi$ at fixed temperature gradient and as the temperature gradient is scanned. In cases where the plasma profiles are pinned to marginal stability and thus $R/L_T$ does not depend directly on the coefficient $\chi_0$, one can consider any shaping effects we find for $\chi_0$ to be indicative of possible shaping effects on $\chi$ in the edge region, which would then improve the core temperature as well by providing a higher edge boundary condition.

## III. JET-BASED PLASMA EQUILIBRIUM

For these shaping studies, we use the local parameterized equilibrium model developed by Miller *et al.*[20] to obtain a realistic treatment of the plasma shape. In the Miller model, nine parameters are required to fully describe the local equilibrium: $\kappa$ (elongation), $\delta$ (triangularity), $\hat{s}$ (global magnetic shear), $\alpha$ (pressure gradient), $R/a$ (aspect ratio), $q$ (safety factor), $\partial_r R_0$, $\partial_r \kappa$, and $\partial_r \delta$. The shape of a flux surface is specified using a standard formula for D-shaped plasmas:

$$R_s = R_0 + r \cos[\theta + (\sin^{-1} \delta)\sin \theta], \tag{3}$$

$$Z_s = \kappa r \sin(\theta). \tag{4}$$

The primary advantage of this model compared with a full numerical equilibrium is that the parameters can be individually varied, thus allowing for systematic studies of the effects of each upon stability and transport for shaped flux surfaces.

A complete scan of a nine-dimensional parameter space as described by the Miller local equilibrium model using
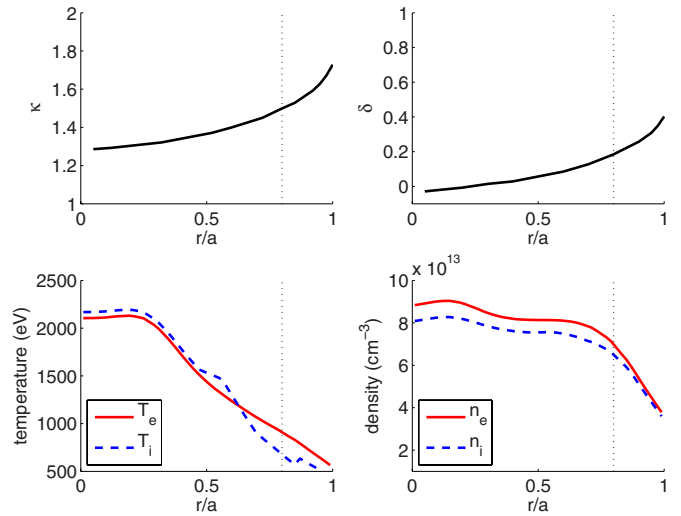


FIG. 1. (Color online) TRANSP analysis of the experimental data from JET ELMy shot 52979, $t=22.0$ s: the radial variation of the elongation $\kappa$, triangularity $\delta$, electron and hydrogenic ion temperatures, and electron and deuterium densities. The dotted vertical lines mark zone 75.

generic equilibria would be difficult due to the computational intensity of nonlinear gyrokinetic simulations. Furthermore, in most real experiments, the various shaping parameters are not fully independent and tend to be correlated with each other. Thus, we consider a single cut through the space of shaping parameters, beginning with parameters from an existing tokamak as a base case. Specifically, our simulation studies begin with shaping parameters based on experimental data from JET.[27] We have focused on JET ELMy shot 52979, $t=22.0$ s. This shot was run as a long duration, high density experiment to study density peaking, as described in Refs. 28 and 29, and is included in the ITER Profile Database.[30] Radial profiles of the shaping parameters and the ion and electron temperatures and densities from TRANSP analysis[31–33] of the data are shown in Fig. 1. We have chosen one radial zone as a representative shaped flux surface and then artificially varied the shaping parameters using the Miller formalism to approach the circular limit via linear interpolations. This zone, which we will refer to as zone 75, corresponds to $r/a=0.80$ and was chosen in particular because shaping effects are strongest near the plasma edge, yet experimental measurements too close to the edge are subject to large uncertainties.

The standard local parameters based on the JET zone 75 equilibrium are given as follows: $r/a=0.80$, $R/a=3.42$, $\partial_r R_0=-0.14$, $q=2.03$, $\hat{s}=1.62$. The original shaping parameters for zone 75 are: $\kappa=1.46$, $\partial_{r/a}\kappa=0.57$, $\delta=0.19$, $\partial_{r/a}\delta=0.60$. We note that here we use a symmetrized geometry for simplicity and thus have neglected the slight up-down asymmetry seen in the actual plasma shape, as this is not accounted for in the standard Miller formalism. The parametrizations of the shaping factors based on linear interpolations of this data are given by

$$\partial_{r/a}\kappa(\kappa) = (0.57/0.46)(\kappa - 1), \tag{5}$$

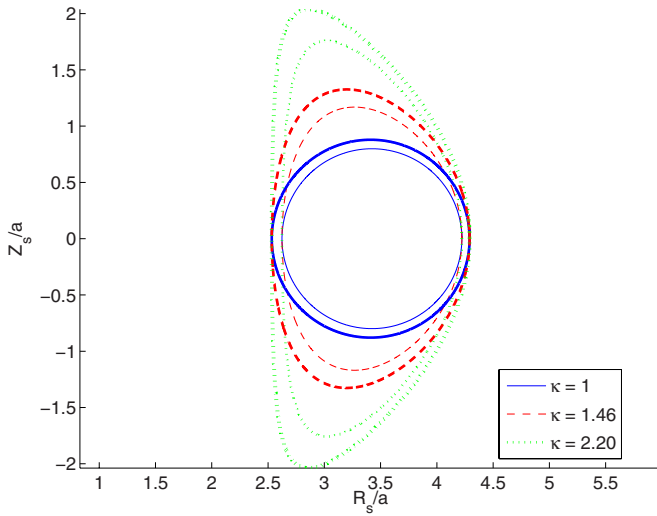$$\delta(\kappa) = (0.19/0.46)(\kappa - 1), \tag{6}$$

FIG. 2. (Color online) Neighboring flux surface shapes for representative JET-like plasmas. The $\kappa=1.46$ case corresponds to the original experimental JET zone 75 equilibrium.
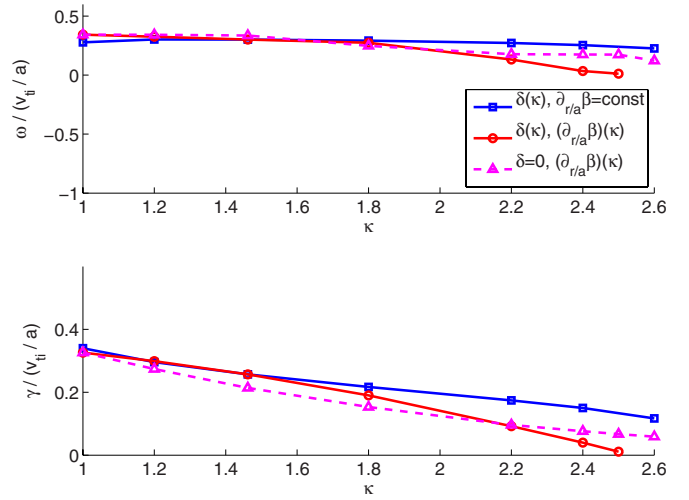


FIG. 3. (Color online) Real frequency and linear growth rate vs elongation comparing zero triangularity and triangularity varied with $\kappa$, as well as comparing constant $\beta$ radial gradient and $\beta$ radial gradient varied with $\kappa$.

$$\partial_{r/a}\delta(\kappa) = (0.60/0.19)\delta(\kappa). \tag{7}$$

Plots of neighboring flux surfaces for the JET-based parameter scan showing the effects of $\kappa$ and $\delta$ on the equilibrium can be seen in Fig. 2. We limit our scan to $\kappa \leq 2.6$ since, in real experiments, tokamaks with very high elongation are subject to the catastrophic MHD vertical instability. In the GS2 simulations, we use a single ion species, thus neglecting impurity species, and include gyrokinetic electrons with the following base case parameters: $T_{0i}=T_{0e}$, $R/L_{Ti}=R/L_{Te}=10.81$, $R/L_{ni}=R/L_{ne}=3.50$, $\nu_{ei}/(v_{ti}/a)=0.393$, and $\nu_{ii}/(v_{ti}/a)=9.88\times10^{-3}$. Here the temperature and density gradient scale lengths are defined as $1/L_{Ts} \doteq -(1/T_{0s}) \times (dT_{0s}/dr)$ and $1/L_{ns} \doteq -(1/n_{0s})(dn_{0s}/dr)$. We note that some smoothing of the data shown in Fig. 1 was done before calculating the local temperature gradients used here, as the kinky behavior seen in the ion temperature profile is due to the effects of the high density of the shot on the diagnostic.

The simulation results presented here are performed in the electrostatic limit ($A_\parallel=0$), yet with finite equilibrium $\beta$ radial gradient (related to the second derivative of the Shafranov shift in the Miller equilibrium model), defined as

$$\partial_{r/a}\beta \doteq \sum_s \partial_{r/a}\beta_s = -\sum_s \beta_s(R/L_{ns}+R/L_{Ts})(a/R), \tag{8}$$

where the total $\beta_{total}$ is given by the sum over the $\beta$ for each species; i.e., $\beta_{total}=\Sigma_s\beta_s$ for $\beta_s \doteq 8\pi n_{0s}T_{0s}/B^2$. The simulations are performed either assuming a fixed value of $\beta$ across shaping parameters at the original zone 75 value, $\beta_{s,\text{zone 75}} = 7.58\times10^{-3}$, denoted as "$\partial_{r/a}\beta=$const." results, or varying $\beta$ with shaping, denoted as "$(\partial_{r/a}\beta)(\kappa)$" results. Comparison between these two cases allows for a study of the effects of the equilibrium generated by the $\beta$ gradient on the dynamics. For the $(\partial_{r/a}\beta)(\kappa)$ results, the variation of $\beta$ with shaping is formulated to keep the Troyon-normalized $\beta$ fixed, $\beta_N \doteq \beta/(I_p/(aB_T))$, while also holding $q_{95}$ fixed. (When electromagnetic perturbations ($\delta A_\parallel$) are included, it is particularly important to reduce $\beta$ as elongation is reduced to the circular

limit in order to avoid running into ballooning limits.) Tokamak reactors are generally designed to work at a fixed value of $\beta_N$ (near the maximum constrained by the stability of pressure-driven modes) and $q_{95}$ (constrained by the stability of kink modes). A scaling for the shaping factor $f_s(\kappa,\delta)$ that relates plasma current to plasma shaping is assumed based on a modification of Uckan's fit to numerical MHD equilibria,[34]

$$\beta_{\text{Troyon}} = \frac{I_p}{aB_T} \propto \frac{a}{Rq_{95}}f_s(\kappa,\delta) = \frac{a}{Rq_{95}}\left[\frac{1+\kappa^2(1+2\delta^2)}{2}\right]. \tag{9}$$

At fixed $q_{95}$, as the plasma elongates, the poloidal current $I_p$ increases. Thus, we vary $\beta$ as

$$\beta_s(\kappa) = \beta_{s,\text{zone 75}}\left[\frac{1+\kappa^2(1+2\delta^2)}{1+\kappa_{\text{zone 75}}^2(1+2\delta_{\text{zone 75}}^2)}\right]. \tag{10}$$

## IV. LINEAR GYROKINETIC STABILITY

We first explore the effects of shaping on the linear gyrokinetic stability. For all of the linear results, we report the maximum linear growth in a scan over $k_y\rho_i$ in the range $0.1 \leq k_y\rho_i \leq 1.0$. Here, $\rho_i=v_{ti}/\Omega_i$ is the ion gyroradius, where $v_{ti}=\sqrt{T_{0i}/m_i}$ is the ion thermal speed and $\Omega_i=Z_ieB/(m_ic)$ is the cyclotron frequency.

We begin with studies of the variation of the linear ITG growth rate with $\kappa$, shown in Fig. 3. In general, the results show that elongation has a stabilizing influence on the linear growth rate. The $\delta=0$ curve is used as a base case comparison with the $\delta(\kappa)$ curve, from which we observe that triangularity is slightly destabilizing at low-to-moderate $\kappa$ and slightly stabilizing at very high $\kappa$. However, the overall dependence of the linear stability on triangularity is very weak compared with the stabilizing effects of elongation. Comparison with the curve at constant $\beta$ radial gradient shows that increasing $-\partial_{r/a}\beta$ is also stabilizing. The stabilizing influence of the $\beta$ gradient has been shown previously and has
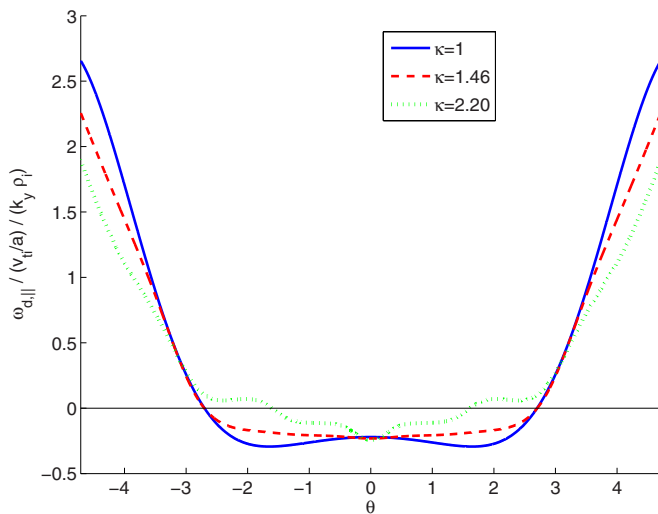
FIG. 4. (Color online) Curvature drift frequency as a function of $\theta$ computed using the Miller formalism for JET-based plasma input parameters. $\omega_{d,\parallel} < 0$ corresponds to drifts in the bad-curvature direction.
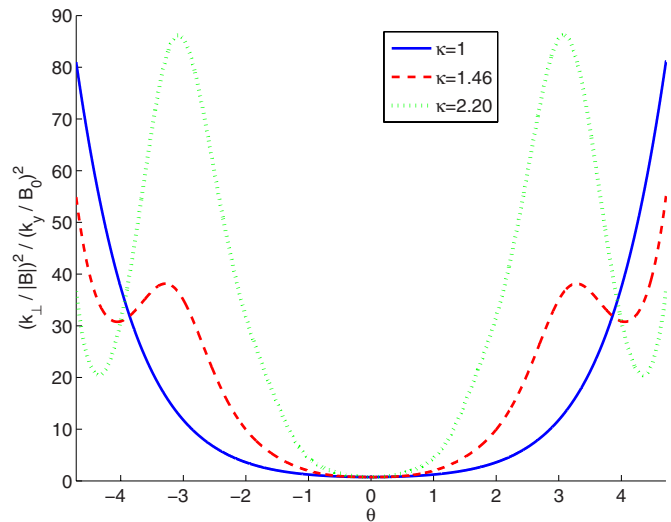


FIG. 5. (Color online) Normalized perpendicular wave number squared as a function of $\theta$ computed using the Miller formalism for JET-based plasma input parameters. FLR averaging becomes important when $k_\perp \rho_i > 1$.

been demonstrated to be particularly important in high-$\beta$ spherical torus plasmas.[35] Specifically, this can be seen intuitively by considering the form of the drift-velocity operator

$$\vec{v}_D \cdot \nabla = i\frac{v_\parallel^2}{v_{ts}^2}\omega_{d,\parallel} + i\frac{\mu B}{v_{ts}^2}\omega_{d,\perp}, \tag{11}$$

where the curvature and $\nabla B$ drift frequencies are given by

$$\omega_{d,\parallel} = (\rho_s v_{ts}/B)\vec{k}_\perp \cdot \vec{B} \times (\hat{b} \cdot \nabla \hat{b}), \tag{12}$$

$$\omega_{d,\perp} = (\rho_s v_{ts}/B^2)\vec{k}_\perp \cdot \vec{B} \times \nabla B. \tag{13}$$

In the high-aspect-ratio limit in circular geometry,

$$\omega_{d,\parallel} = -\left(\frac{k_y \rho_s v_{ts}}{R_0}\right)[\cos\theta + (\hat{s}\theta - \alpha\sin\theta)\sin\theta], \tag{14}$$

$$\omega_{d,\perp} = \omega_{d,\parallel} + \left(\frac{k_y \rho_s v_{ts}}{R_0}\right)\frac{\alpha}{2q^2}, \tag{15}$$

where $\alpha \doteq -q^2(R_0/a)\partial_{r/a}\beta$ is related to the second derivative of the Shafranov shift and $\omega_{d,\parallel} < 0$ corresponds to drifts in the bad-curvature direction. Thus, Eq. (14) shows that the stabilizing effect of increased $-\partial_{r/a}\beta$ (or equivalently increased $\alpha$) is analogous to that due to reversed local magnetic shear. We note that, while the magnetic field curvature is the main source of the bad-curvature instability drive, there appears to also be some stabilizing effect of $\alpha$ in the $\nabla B$ drift in Eq. (15). However, this is offset by other effects when compressibility ($\delta B_\perp$) is included.

Insight about the stabilizing effects of high shaping observed in Fig. 3 can similarly be obtained by considering the more general equilibrium. Figure 4 shows the variation of the curvature drift frequency with the ballooning mode extended angle $\theta$ for the JET-based plasmas ($\delta$ is also varied with $\kappa$ here). In general, moderate levels of shaping appear to have little effect on the curvature drift. However, the case of $\kappa = 2.20$ shows a significantly more narrow region in the bad-curvature direction. Thus, with high shaping, only un-

stable modes which are very highly localized along the field line will persist in the system. This will have a stabilizing influence, since these narrow eigenmodes will contain higher $k_\parallel$ components, which are subject to Landau damping in the local limit. Another stabilizing effect is due to the variation of the perpendicular wave number $k_\perp(\theta)$ shown in Fig. 5. In the concentric-circle high-aspect-ratio limit, $k_\perp^2 = k_y^2 + k_x^2 = k_y^2(1 + \hat{s}^2(\theta - \theta_0)^2)$ increases along the field line (away from the point $\theta_0$ where the radial wave number vanishes, $\theta_0 = 0$ here). This is because an eigenmode in the ballooning representation follows the sheared magnetic field. Noncircular shaping induces additional stretching and shearing of a flux tube that can also increase $k_\perp^2$, as shown in Fig. 5. The resulting finite Larmor radius (FLR) averaging by ions at high $k_\perp \rho_i$ and the associated further narrowing of the eigenmode along the field line will also contribute to the stabilizing influence seen with stronger shaping. On a related note, we also consider the variation of the Jacobian factor $\mathcal{J}$ associated with the parallel motion operator, $\hat{b} \cdot \nabla = (1/\mathcal{J})\partial/\partial\theta$. Freedom in the definition of $\theta$ has been exploited to remove the $\theta$ dependence from $\mathcal{J}$. For these parameters, we find that $a/\mathcal{J} = \{0.149, 0.152, 0.157\}$ for the cases of $\{\kappa = 1, \kappa = 1.46, \kappa = 2.20\}$, thus indicating a slightly higher amount of stabilizing Landau damping with increased shaping.

The effects of shaping on the linear critical temperature gradient were also studied. The results are shown in Fig. 6. Here, $\partial_{r/a}\beta$ is varied with shaping ($\kappa$ and $\delta$) as well as consistently with $R/L_T$. While shaping was found to be stabilizing in the regime of $R/L_T = 10.81$ in Fig. 3, here we find surprisingly that shaping has no significant effect on the linear critical temperature gradient. Specifically, all three shaped plasmas yield a stabilizing gradient for the ITG mode near that observed for the circular shape; i.e., $(R/L_T)_{\mathrm{crit}} \sim 3.42$. For comparison, the dashed lines in Fig. 6 for the $\kappa = 1.46$ and $\kappa = 2.20$ cases correspond to constant zero triangularity (rather than varying triangularity with $\kappa$ as for the solid lines). Again we see that the dependence of the ITG
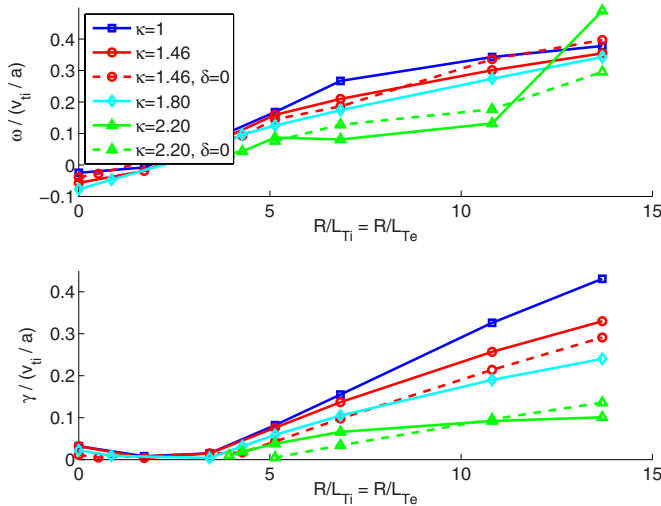
FIG. 6. (Color online) Real frequency and linear growth rate vs temperature gradient scale length. The solid lines correspond to results from varying triangularity with $\kappa$, while the dashed lines correspond to zero triangularity.



FIG. 7. (Color online) Ion and electron heat fluxes vs elongation comparing zero triangularity and triangularity varied with $\kappa$, as well as comparing constant $\beta$ radial gradient and $\beta$ radial gradient varied with $\kappa$. The dotted lines show the empirical scalings $\kappa^{-1}$, $\kappa^{-1.5}$, and $\kappa^{-2}$.

growth rate on $\delta$ is insignificant across the entire temperature gradient scale length regime, except for the upshift in the linear critical temperature gradient with zero triangularity for the $\kappa=2.20$ case.

## V. NONLINEAR ITG TURBULENCE

Extensions to study the scaling of nonlinear turbulence with shaping have also been explored. The simulation domain for these studies has $L_x=74.28\rho_i$ and $L_y=62.83\rho_i$ with the number of grid points in the perpendicular directions given by $N_x=72$ and $N_y=36$, such that $\Delta x=1.05\rho_i$ and $\Delta y=1.80\rho_i$. In spectral space, this corresponds to resolving nonzero modes in the range $0.085 \leqslant |k_x\rho_i| \leqslant 1.95$ and $0.10 \leqslant k_y\rho_i \leqslant 1.10$. The domain along the field line has length $L_z=2\pi qR=12.75R$, with $N_\theta=32$ grid points per $2\pi$ in $\theta$. The velocity grid has $N_E=16$ energy grid points and $N_\lambda=37$ pitch angle grid points ($\lambda=\mu/E$), divided into trapped and untrapped regions. The simulations were performed as typical with time-centering parameter $r=0.55$ and slight upwind diffusion (spatial-centering parameter $s=0.55$).[24] The heat diffusivities presented here are written in terms of $\chi_{\text{ITER}}$, a quantity defined by the ITER Expert Group such that the one-dimensional radial heat transport equation is given by

$$\frac{3}{2}\frac{\partial(nT)}{\partial t} = \frac{1}{V'}\frac{\partial}{\partial r}\left[V'\langle|\nabla r|^2\rangle\chi_{\text{ITER}}\left(n\frac{\partial T}{\partial r}\right)\right] + S_E, \qquad (16)$$

where $V$ is the flux-surface volume, $V' \doteq dV/dr$, and $S_E$ is the energy source term. The transport equation in this form has the advantage that $\chi_{\text{ITER}}$ is independent of the flux surface label $r$.

### A. Transport scalings

The effects of shaping on the nonlinear ITG turbulence for the JET-based plasmas, analogous with the linear results in Fig. 3, are shown in Fig. 7. In agreement with the linear results, the nonlinear results show that high shaping has a stabilizing influence. Also similar to the linear stability is
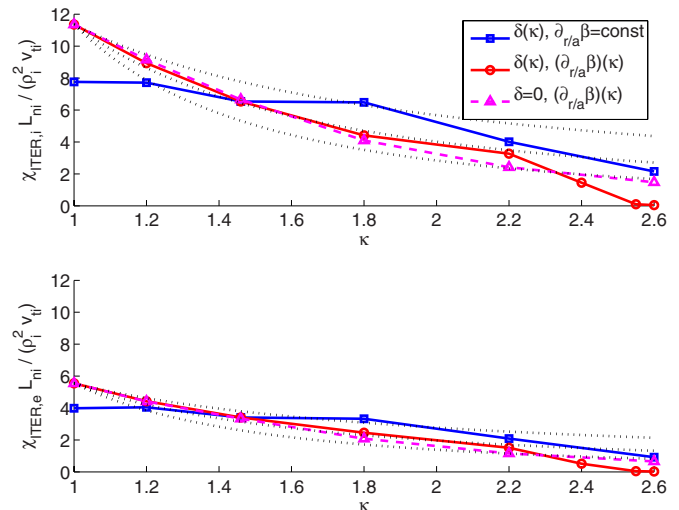
that the dependence of the nonlinear heat flux on triangularity is weak across the entire range. We note further that the results at constant $\beta$ radial gradient do not vary as strongly with $\kappa$, indicating that a significant fraction of the variation of the standard case $\{\delta(\kappa),(\partial_{r/a}\beta)(\kappa)\}$ is coming from the variation of $\partial_{r/a}\beta$ as given by Eq. (10). Comparisons of the GS2 data with the empirical scalings of $\kappa^{-1}$, $\kappa^{-1.5}$, and $\kappa^{-2}$, designed to fit the data at $\kappa=1$, are also shown in Fig. 7. Qualitatively, we find that both the ion and electron heat fluxes scale as $\chi \sim \kappa^{-1.5}$. It is further interesting that, in the regime where triangularity is slightly destabilizing, the scaling of the case with zero triangularity becomes stronger: $\chi \sim \kappa^{-2}$.

Compared with previous numerical studies, the simulation results in Fig. 7 are within the range of the gyrofluid results of Waltz and Miller,[16] who found a scaling of $\chi \sim 2/(1+\kappa^2)$, for $\delta=0$ and adiabatic electrons. However, our nonlinear gyrokinetic simulations of core turbulence do not completely explain the much stronger effects of shaping found experimentally, particularly the strong triangularity dependence observed in tokamaks. For example, in Fig. 8, we show the scaling of $1/\chi$ with $\kappa$ from various experimentally-based empirical scaling relations in comparison with the scalings of $1/\chi \sim \kappa^{1.5}$ and $\kappa^{2.0}$ observed in our GS2 simulations. For the empirical energy confinement time scalings, we assume that $\tau_E \sim a^2/\chi$ and convert the empirical scalings from engineering variables, i.e., $\tau_E \propto I_p^{c_1}P^{c_2}...$, to physics variables for comparison with the gyro-Bohm normalized simulation results. (For example, we eliminate the heating power in terms of the average plasma energy density using $P=W/\tau_E \propto VnT/\tau_E$.) Note that shaping effects are much stronger when $\tau_E$ is expressed in terms of physics variables instead of engineering variables. For example, if $\tau_E \propto I_p P^{-2/3}\kappa^{1/2}$ in engineering variables, then eliminating the power leads to $\tau_E \propto I_p^3\kappa^{3/2}/W^2 \propto [1+\kappa^2(1+2\delta^2)]^3/\kappa^{1/2}$ [using $V \propto \kappa$ and using Eq. (9) to relate $I_p$ to shaping at fixed $q_{95}$ and fixed $B_T$]. The scaling laws which we plot in Fig. 8 include
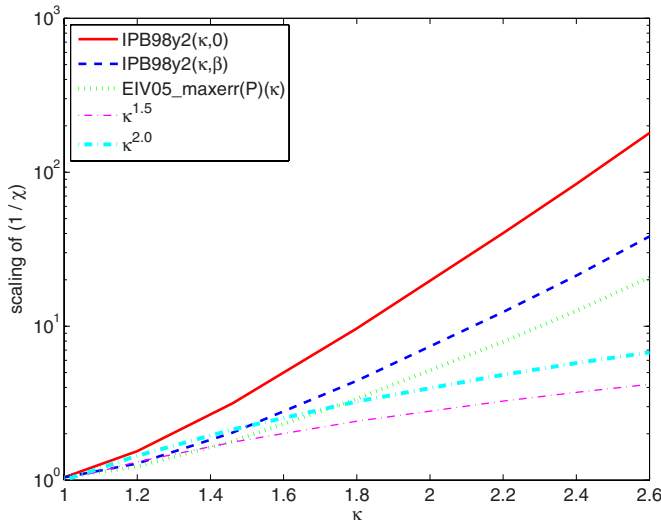
FIG. 8. (Color online) Inverse heat flux vs $\kappa$ (assuming triangularity varies with $\kappa$) for various experimentally-based empirical scaling laws; namely, the standard IPB98(y,2) H-mode scaling for $\beta$=const. ["IPB98y2($\kappa$,0)"] and for $\beta/\beta_{\text{Troyon}}$=const. ["IPB98y2($\kappa,\beta$)"] and the standard Error in Variables scaling ["EIV05maxerr(P)($\kappa$)"]. For comparison, the scalings of $\kappa^{1.5}$ and $\kappa^{2.0}$ (observed in our GS2 simulations) are shown.



FIG. 9. (Color online) Ion and electron heat fluxes vs temperature gradient scale length for triangularity varied with $\kappa$.

the standard IPB98(y,2) scaling,[1] which is based on H-mode global confinement data and was used for the ITER design, for both $\beta$=const. ["IPB98y2($\kappa$,0)"] and $\beta/\beta_{\text{Troyon}}$=const. ["IPB98y2($\kappa,\beta$)"] and the standard Error in Variables scaling[2] ["EIV05_maxerr(P)($\kappa$)"], which is similar to the IPB98(y,2) scaling yet uses a modified H-mode database, resulting in a weaker $\beta$ dependence. While there are significant differences between the shaping dependencies of these three empirical scalings, it is clear from Fig. 8 that our GS2 simulations yield a weaker scaling than the experiments and thus do not fully capture the strong stabilizing effects of highly shaped plasmas. However, note that this analysis neglects marginal stability effects. If pinned to marginal stability, then the energy confinement time $\tau_E$ depends on $(R/L_T)_{\text{crit}}$ and the edge boundary conditions, not on $\chi$ at fixed $R/L_T$, as discussed in Sec. II. The fact that the Dimits nonlinear critical temperature gradient shift depends on shaping, which we observed with the GS2 simulations and show next, may help to explain some of the remaining shaping dependence of the experiments. However, it may be that much of the shaping dependence in tokamaks comes in through edge boundary conditions for core turbulence. In fact, recent work by Kendl and Scott[21] exploring the effects of shaping on plasma turbulence for edgelike parameters using gyrofluid simulations shows a scaling of $\chi \sim \kappa^{-4}$, which is much stronger than we found with our core gyrokinetic simulations. Thus, this will be a key topic of future research. Within this, a number of particular differences between core and edge turbulence, such as the stronger role played by nonlinear, nonadiabatic electron dynamics in edge turbulence, could be interesting to explore further.
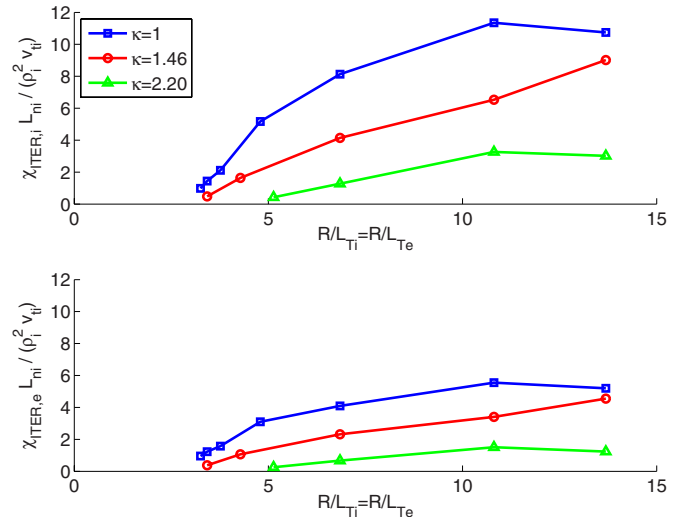
## B. Critical temperature gradient and residual zonal flows

Here we present results from studies of the effects of shaping on the nonlinear critical temperature gradient. The GS2 simulation results are shown in Fig. 9. While shaping was found to be stabilizing on the nonlinear ITG turbulence in the regime of $R/L_T$=10.81 in Fig. 7, in agreement with the linear results, here we find that shaping is also stabilizing near the regime of zero net heat flux. In particular, the results show that the nonlinear critical temperature gradient increases with strong shaping. For example, $(R/L_T)_{\text{crit}} \sim 3.42$ for the $\kappa$=1 and $\kappa$=1.46 cases, while $(R/L_T)_{\text{crit}} \sim 5.13$ for the $\kappa$=2.20 case. This is unlike the linear results in Fig. 6, which showed that shaping has little effect on the linear critical temperature gradient.

The results of Fig. 9 are somewhat surprising and worthy of further analysis. Here we will show that the larger upshift of the nonlinear critical temperature gradient with higher shaping may be due to enhanced zonal flows. Zonal flows are axisymmetric, primarily $m$=0 flows driven by ITG turbulence which are believed to play an important role in saturating the level of the turbulence.[36–38] Rosenbluth and Hinton found analytically that a component of the zonal flows is undamped by linear collisionless processes and that the residual amplitude of these flows scales as

$$\frac{\Phi_f}{\Phi_0} = \frac{1}{1 + \dfrac{1.6}{h}}, \qquad (17)$$

where $h = \sqrt{\varepsilon}/q^2$ (where $\varepsilon = r/R$ is the inverse aspect ratio).[39] This result was derived for concentric-circular plasmas. However, $h$ is related to the physics of banana widths, which depends on the poloidal magnetic field, and thus it is intuitive that $h$ should scale with the shaping parameters.

Physically, what we are considering here is the bounce-averaged gyrokinetic response of the plasma to shield an externally-imposed electrostatic potential $\Phi$. The usual classical gyroradius shielding comes from the ion polarization
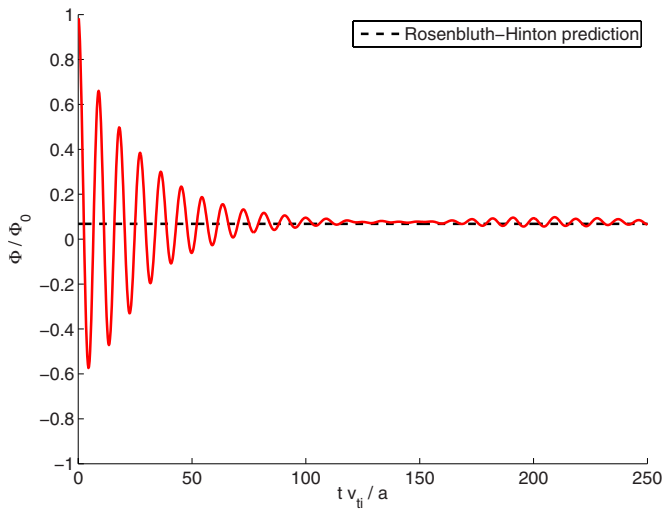
FIG. 10. (Color online) Time evolution of the amplitude of the zonal flows for the JET-based circular case computed using GS2 with an initial external potential $\Phi_{\text{ext}} \sim (1/k_r)\cos(k_r r)$. The dashed line shows the Rosenbluth-Hinton prediction for the saturated potential for these parameters.
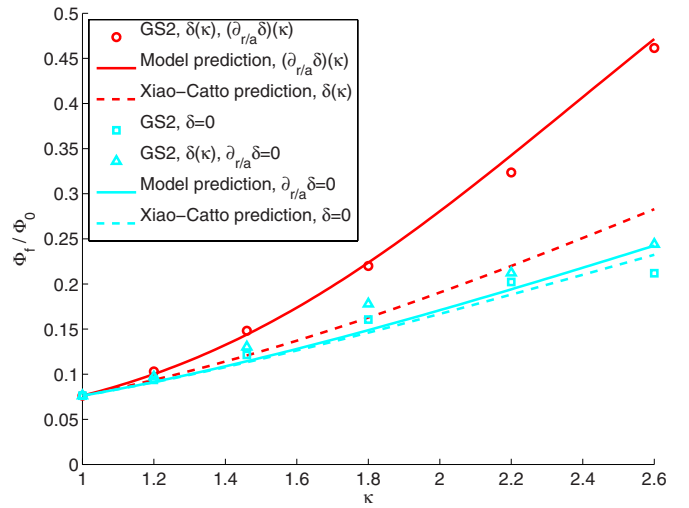


FIG. 11. (Color online) Amplitude of the Rosenbluth-Hinton residual zonal flows vs elongation comparing triangularity and its radial gradient varied with $\kappa$, zero triangularity, and triangularity varied with $\kappa$ with zero triangularity radial gradient. The data points are the GS2 results, the solid lines are our model prediction, and the dashed lines are the analytic model of Xiao and Catto (with $\Delta = 0$).

density term, proportional to $[1 - \Gamma_0(k_\perp^2 \rho_i^2)]$ in the gyrokinetic Poisson equation. Thus, in the limit of small $k_\perp \rho_i$, the classical perpendicular plasma dielectric can be approximated as $D_{\text{classical}} \sim 1 + \rho_i^2/\lambda_{Di}^2 \sim \rho_i^2/\lambda_{Di}^2 \gg 1$, where $\lambda_{Di}^2 \doteq T_{0i}/(4\pi n_{0i} Z_i e^2)$ is the square of the Debye length. This shielding effect is set up in a short time, after a few gyroperiods. In the long time limit, after a few bounce times, neoclassical polarization shielding also arises due to the distortion of the banana orbits by the radial electric field. Thus, the neoclassical perpendicular plasma dielectric scales as $D_{\text{neoclassical}} \sim (\rho_{\text{banana}}^2/\lambda_{Di}^2)f_{\text{trapped}}$, where $\rho_{\text{banana}} \sim \rho_i q/\sqrt{\epsilon}$ is the banana-orbit width and $f_{\text{trapped}} \sim \sqrt{\epsilon}$ is the fraction of trapped particles (representing the fact that trapped particles have larger radial excursions off a flux surface than passing particles). Thus, we find that $D_{\text{neoclassical}}/D_{\text{classical}} \sim q^2/\sqrt{\epsilon} = 1/h$. Assuming an initial $\Phi$ due only to the classical polarization density, in the long time limit considered by Rosenbluth and Hinton (i.e., $\omega \ll \omega_{\text{bounce}}$), $\Phi$ will be reduced due to the neoclassical enhancement of polarization shielding by a factor of $D_{\text{classical}}/(D_{\text{neoclassical}} + D_{\text{classical}})$, which we find scales as $\sim 1/(1 + 1/h)$, in qualitative agreement with the Rosenbluth-Hinton result given in Eq. (17). (The factor of 1.6 in Eq. (17) comes from a more accurate kinetic calculation which also includes the contribution of passing particles.) In physical terms, in the time evolution, the amplitude of the potential appears as the superposition of transit-time damping oscillations, known as the geodesic acoustic modes, and an undamped residual component, which we refer to as the Rosenbluth-Hinton component of the zonal flows. This is shown in Fig. 10.

With this picture of the neoclassical enhancement of polarization shielding, we can now see how shaping can enhance the Dimits nonlinear shift: increasing the plasma elongation allows the current to go up (at fixed $q_{95}$ and $B_T$), which increases the poloidal flux and makes the banana

widths thinner, which reduces the neoclassical shielding of zonal flows and thus produces a larger Dimits shift in the critical temperature gradient.

We now numerically explore the effects of shaping on the Rosenbluth-Hinton residual flows, focusing specifically on the dependence of $h$ on shaping. Using GS2, we find the amplitude of the Rosenbluth-Hinton residual flows by adding an external $\Phi$ to the gyrokinetic Poisson equation and then computing the response of the plasma to it. Figure 11 shows the results; specifically, the saturated amplitude of the Rosenbluth-Hinton residual zonal flows versus $\kappa$ for the JET-based parameters. Overall, we find that shaping enhances the Rosenbluth-Hinton component of the zonal flows. This provides an explanation for the larger upshift of the nonlinear critical temperature gradient with higher shaping observed in Fig. 9, since zonal flows help to saturate the turbulence. From Fig. 11, we note that the results with triangularity varied with elongation show stronger residual zonal flow levels than results with zero triangularity. However, comparison with results using zero triangularity radial gradient shows that it is the increased $\partial_{r/a}\delta$, rather than $\delta$ itself, that is having the most significant stabilizing effect. For all cases, increased elongation (with increased elongation radial gradient) is favorable.

A model prediction for the scaling of $h$ with shaping can be found empirically based on these GS2 results. We assume the following form of the residual amplitude:

$$\frac{\Phi_f}{\Phi_0} = \frac{1}{1 + \dfrac{1.6}{C h_{\text{shaping}}}}, \tag{18}$$

where

$$h_{\text{shaping}} = \frac{\sqrt{\epsilon}}{q^2} f(\kappa, \delta). \tag{19}$$

The constant $C=0.887$ is chosen to match the GS2 circular case with the original Rosenbluth-Hinton model. (Note that the Rosenbluth-Hinton analyis assumes concentric-circular plasmas, while our JET-based plasmas have a nonzero Shafranov shift.) A good fit is found with the shaping function

$$f(\kappa,\delta) = \frac{1}{2}\left[ 1 + \kappa^2\left( 1 + \frac{1}{2}\frac{r}{a}\partial_{r/a}\delta \right)^2 \right], \qquad (20)$$

where the functional form of the triangularity term comes from the scaling $\partial_{r/a}\delta \sim 2\delta/(r/a)$ to reflect the observed strong radial gradient dependence. This is shown as the solid lines in Fig. 11. Note the good agreement between the GS2 results and the model prediction both with zero triangularity gradient and with triangularity varied with $\kappa$. It is interesting to compare this shaping function with that found empirically based on experiments for the pressure limit, such as the Troyon $\beta$ limit given by Eq. (9). The shaping function of Eq. (20) for the residual zonal flows has a similar $\kappa$ dependence as the empirical Troyon $\beta$ limit, yet with a slightly weaker $\delta$ dependence.

Figure 11 also shows a comparison between the GS2 results and a recent analytic extension of the Rosenbluth-Hinton calculation by Xiao and Catto[40] to include shaping effects, which was motivated by our numerical results and model prediction, which were obtained first.[41] The Xiao-Catto analytic model is based on a simple global analytic equilibrium solution of the Grad-Shafranov equation using an inverse-aspect-ratio expansion. Here we plot their results at Shafranov shift $\Delta=0$, rescaling their shaping function $f(\kappa,\delta)$ to match the GS2 JET-based circular result. (It is the radial gradient of the Shafranov shift, rather than the Shafranov shift itself, which can have a significant effect on gyrokinetics, causing an enhancement of the magnetic field at the outer boundary due to the squeezing of adjacent flux surfaces.) While the analytic approximation is in good agreement with the GS2 results at $\delta=0$, the Xiao-Catto $\delta(\kappa)$ result is much weaker, closer to our zero triangularity gradient results. This difference is most likely the result of an assumed weaker $\delta$ radial profile in the simplified global analytic equilibrium used in the analytic theory. Specifically, the Xiao-Catto model corresponds to a particular parameterization of an equilibrium with an assumed pressure and current profile (constant $dp/d\psi$ and constant $IdI/d\psi$). The value $\partial_{r/a}\delta$ at a particular minor radius depends in a nonlocal way on the pressure and current profiles inside that radius, just as the Shafranov shift gradient in a shifted-circular equilibrium depends on integrals of the pressure and poloidal magnetic field; i.e., $\partial_r\Delta = -(r/R_0)(\beta_p + \ell_i/2)$. While the simple analytic global equilibrium used in the Xiao-Catto model cannot reproduce every possible local equilibrium that we can set up with the Miller model, the parameters of the Miller equilibrium could be chosen to locally match any assumed global analytic equilibrium, so that the Xiao-Catto analytic result can be used as a benchmark to verify that a code properly reproduces this physics. In fact, Xiao *et al.*[42] subsequently carried out this test successfully with GS2. Here, however, we have not determined the global pressure and poloidal field profiles required to obtain a particular local triangularity gradient, although we have shown with our GS2 results that the residual zonal flows depend sensitively on the resulting $\partial_{r/a}\delta$. Nevertheless, the Xiao-Catto analytic theory generally confirms our numerical results for the elongation dependence.

Overall, this analysis has shown that the observed increase in the Dimits nonlinear critical temperature gradient shift with plasma shaping in Fig. 9 may be understood as an enhancement of the residual zonal flows with plasma shaping, and this may help to explain why strong shaping is favorable in experiments.

## VI. DISCUSSION AND SUMMARY

The GS2 code has been used to study the effects of flux surface shape on the gyrokinetic stability and transport of tokamak plasmas. Studies of the scaling of the linear growth rate and nonlinear turbulence with shaping parameters were performed starting with a representative JET-like flux surface and artificially varying elongation, triangularity, and their radial gradients together using the analytic Miller local equilibrium model to approach the circular limit via linear interpolation. In the electrostatic limit, high elongation was found to have a stabilizing influence on both the linear ITG instability and the nonlinear ITG turbulence. Triangularity was somewhat destabilizing at moderate $\kappa$, but could be stabilizing at high $\kappa$. A general scaling of the heat flux with elongation of $\chi \sim \kappa^{-1.5}$ was found for the nonlinear turbulence levels, with a slightly stronger scaling of $\chi \sim \kappa^{-2}$ with zero triangularity in the high-$\kappa$ regime where triangularity is destabilizing. This scaling is consistent with previous gyrofluid simulations. Investigations of the effects of shaping on the critical temperature gradient showed that, while shaping had little effect on the linear critical temperature gradient, high shaping resulted in a larger upshift of the nonlinear critical temperature gradient due to enhanced zonal flows.

Overall, while our nonlinear gyrokinetic simulations of core turbulence capture some of the shaping effects found experimentally, they do not completely explain the degree of this dependence on shaping, particularly the strong triangularity dependence observed in tokamaks. While the result that the Dimits nonlinear shift is enhanced with shaping may help to further explain why shaping is favorable in experiments, it may be that much of the experimentally observed strong triangularity dependence comes from the edge turbulence, which sets the boundary conditions for core turbulence and transport. This will be explored in future research. The edge region is particularly complicated due to the existence of both weak and strong collisionality regimes, steep gradients such that particle drift-orbit widths can be comparable to the equilibrium radial gradient scale lengths, open and closed field lines, wall interactions, strong atomic physics effects, etc. Thus, most edge plasma simulations are presently done with fluid simulation models, such as the BOUT code[43] and GEM code,[22,23] although initiatives to develop new gyrokinetic codes to specifically simulate edge turbulence are underway. However, along these lines, extensions of our results to include electromagnetic dynamics are in progress and may

be of interest for further shaping studies of edgelike plasmas, since electromagnetic dynamics are particularly significant in the edge region due to the high pressure gradient. Previous studies of MHD stability for highly shaped edgelike plasmas show that high triangularity can give improved access to the second stability regime.[20]

Finally, a more complete understanding of shaping effects might also include scanning shaping parameters over a range of values of $q$, as some previous gyrofluid work suggests that there is a stronger $\kappa$ dependence at lower $q$.[16] Exploration of higher-degree shaping moments such as squareness $\zeta$, which modifies the D-shaped plasma formulae in Eqs. (3) and (4) by $Z_s \rightarrow \kappa r[\sin(\theta) + \zeta \sin(2\theta)]$, may also be of interest, since $\zeta$ has been found to have a significant stabilizing effect in some DIII-D experiments[44,45] and in MHD studies.[46]

## ACKNOWLEDGMENTS

[1]ITER Physics Expert Group on Confinement and Transport, ITER Physics Expert Group on Confinement Modelling and Database, and ITER Physics Basis Editors, Nucl. Fusion **39**, 2175 (1999).

[2]J. G. Cordey, K. Thomsen, A. Chudnovsky, O. J. W. F. Kardaun, T. Takizuka, J. A. Snipes, M. Greenwald, L. Sugiyama, F. Ryter, A. Kus, J. Stober, J. C. DeBoo, C. C. Petty, G. Bracco, M. Romanelli, Z. Cui, Y. Liu, D. C. McDonald, A. Meakins, Y. Miura, K. Shinohara, K. Tsuzuki, Y. Kamada, H. Urano, M. Valovic, R. Akers, C. Brickley, A. Sykes, M. J. Walsh, S. M. Kaye, C. Bush, D. Hogewei, Y. Martin, A. Cote, G. Pacher, J. Ongena, F. Imbeaux, G. T. Hoang, S. Lebedev, and V. Leonov, Nucl. Fusion **45**, 1078 (2005).

[3]F. Troyon, R. Gruber, H. Saurenmann, S. Semenzato, and S. Succi, Plasma Phys. Controlled Fusion **26**, 209 (1984).

[4]M. Greenwald, Plasma Phys. Controlled Fusion **44**, R27 (2002).

[5]E. A. Lazarus, M. S. Chu, J. R. Ferron, F. J. Helton, J. T. Hogan, A. G. Kellman, L. L. Lao, J. B. Lister, T. H. Osborne, R. Snider, E. J. Strait, T. S. Taylor, and A. D. Turnbull, Phys. Fluids B **3**, 2220 (1991).

[6]J. R. Ferron, T. A. Casper, E. J. Doyle, A. M. Garofalo, P. Gohil, C. M. Greenfield, A. W. Hyatt, R. J. Jayakumar, C. Kessel, J. Y. Kim, T. C. Luce, M. A. Makowski, J. Menard, M. Murakami, C. C. Petty, P. A. Politzer, T. S. Taylor, and M. R. Wade, Phys. Plasmas **12**, 056126 (2005).

[7]J. Ongena, W. Suttrop, M. Becoulet, G. Cordey, P. Dumortier, Th. Eich, L. C. Ingesson, S. Jachmich, P. Lang, A. Loarte, P. Lomas, G. P. Maddison, A. Messiaen, M. F. F. Nave, J. Rapp, G. Saibene, R. Sartori, O. Sauter, J. D. Strachan, B. Unterberg, M. Valovic, B. Alper, Ph. Andrew, Y. Baranov, J. Brzozowski, J. Bucalossi, M. Brix, R. Budny, M. Charlet, I. Coffey, M. De Baar, P. De Vries, C. Gowers, N. Hawkes, M. von Hellermann, D. L. Hillis, J. Hogan, G. L. Jackson, E. Joffrin, C. Jupen, A. Kallenbach, H. R. Koslowski, K. D. Lawson, M. Mantsinen, G. Matthews, P. Monier-Garbet, D. McDonald, F. Milani, M. Murakami, A. Murari, R. Neu, V. Parail, S. Podda, M. E. Puiatti, E. Righi, F. Sartori, Y. Sarazin, A. Staebler, M. Stamp, G. Telesca, M. Valisa, B. Weyssow, K.-D. Zastrow, and

EFDA-JET Workprogramme Contributors, Plasma Phys. Controlled Fusion **43**, A11 (2001).

[8]A. Pochelon, T. P. Goodman, M. Henderson, C. Angioni, R. Behn, S. Coda, F. Hofmann, J.-P. Hogge, N. Kirneva, A. A. Martynova, J.-M. Moret, Z. A. Pietrzyk, F. Porcellib, H. Reimerdes, J. Rommers, E. Rossib, O. Sauter, M. Q. Tran, H. Weisen, S. Alberti, S. Barry, P. Blanchard, P. Bosshard, R. Chavan, B. P. Duval, Y. V. Esipchucka, D. Fasel, A. Favre, S. Franke, I. Furno, P. Gorgerat, P.-F. Isoz, B. Joye, J. B. Lister, X. Llobet, J.-C. Magnin, P. Mandrin, A. Manini, B. Marl'etaz, P. Marmillod, Y. Martin, J.-M. Mayor, J. Mlynar, C. Nieswand, P. J. Paris, A. Perez, R. A. Pitts, K. A. Razumovaa, A. Refke, E. Scavino, A. Sushkova, G. Tonetti, F. Troyon, W. Van Toledo, and P. Vyas, Nucl. Fusion **39**, 1807 (1999).

[9]C. Kessel, J. Manickam, G. Rewoldt, and W. M. Tang, Phys. Rev. Lett. **72**, 1212 (1994).

[10]T. M. Antonsen, J. F. Drake, P. N. Guzdar, A. B. Hassam, Y. T. Lau, C. S. Liu, and S. V. Novakovskii, Phys. Plasmas **3**, 2221 (1996).

[11]B. Coppi, A. Ferreira, J. W. K. Mark, and J. J. Ramos, Nucl. Fusion **19**, 715 (1979).

[12]S. C. Jardin, C. E. Kessel, T. K. Mau, R. L. Miller, F. Najmabadi, V. S. Chan, M. S. Chu, R. LaHaye, L. L. Lao, T. W. Petrie, P. Politzer, H. E. St. John, P. Snyder, G. M. Staebler, A. D. Turnbull, and W. P. West, Fusion Eng. Des. **80**, 25 (2005).

[13]S. C. Jardin, C. E. Kessel, C. G. Bathke, D. A. Ehst, T. K. Mau, F. Najmabadi, T. W. Petrie, and the ARIES Team, Fusion Eng. Des. **38**, 27 (1997).

[14]G. Rewoldt, W. M. Tang, and M. S. Chance, Phys. Fluids **25**, 480 (1982).

[15]D. D. Hua, X. Q. Xu, and T. K. Fowler, Phys. Fluids B **4**, 3216 (1992).

[16]R. E. Waltz and R. L. Miller, Phys. Plasmas **6**, 4265 (1999).

[17]D. R. Ernst, P. T. Bonoli, P. J. Catto, W. Dorland, C. L. Fiore, R. S. Granetz, M. Greenwald, A. E. Hubbard, M. Porkolab, M. H. Redi, J. E. Rice, K. Zhurovich, and Alcator C-Mod Group, Phys. Plasmas **11**, 2637 (2004).

[18]J. E. Kinsey, R. E. Waltz, and J. Candy, Phys. Plasmas **14**, 102306 (2007).

[19]Y. Chen, S. E. Parker, G. Rewoldt, S. H. Ku, G. Y. Park, and C. S. Chang, Phys. Plasmas **15**, 055905 (2008).

[20]R. L. Miller, M. S. Chu, J. M. Greene, Y. R. Lin-Liu, and R. E. Waltz, Phys. Plasmas **5**, 973 (1998).

[21]A. Kendl and B. D. Scott, Phys. Plasmas **13**, 012504 (2006).

[22]B. Scott, Phys. Plasmas **7**, 1845 (2000).

[23]B. Scott, Phys. Plasmas **12**, 102307 (2005).

[24]M. Kotschenreuther, G. Rewoldt, and W. M. Tang, Comput. Phys. Commun. **88**, 128 (1995).

[25]W. Dorland, F. Jenko, M. Kotschenreuther, and B. N. Rogers, Phys. Rev. Lett. **85**, 5579 (2000).

[26]M. Kotschenreuther, W. Dorland, M. A. Beer, and G. W. Hammett, Phys. Plasmas **2**, 2381 (1995).

[27]P. H. Rebut and B. E. Keen, Fusion Technol. **11**, 13 (1987).

[28]M. Valovic, J. Rapp, J. G. Cordey, R. Budny, D. C. McDonald, L. Garzotti, A. Kallenbach, M. A. Mahdavi, M. A. Mahdavi, J. Ongena, V. Parail, G. Saibene, R. Sartori, M. Stamp, O. Sauter, J. Strachan, W. Suttrop, and Contributors to the EFDA-JET Workprogramme, Plasma Phys. Controlled Fusion **44**, 1911 (2002).

[29]J. Ongena, P. Monier-Garbet, W. Suttrop, Ph. Andrew, M. B'ecoulet, R. Budny, Y. Corre, G. Cordey, P. Dumortier, Th. Eich, L. Garzotti, D. L. Hillis, J. Hogan, L. C. Ingesson, S. Jachmich, E. Joffrin, P. Lang, A. Loarte, P. Lomas, G. P. Maddison, D. McDonald, A. Messiaen, M. F. F. Nave, G. Saibene, R. Sartori, O. Sauter, J. D. Strachan, B. Unterberg, M. Valovic, I. Voitsekhovitch, M. von Hellermann, B. Alper, Y. Baranov, M. Beurskens, G. Bonheure, J. Brzozowski, J. Bucalossi, M. Brix, M. Charlet, I. Coffey, M. De Baar, P. De Vries, C. Giroud, C. Gowers, N. Hawkes, G. L. Jackson, C. Jupen, A. Kallenbach, H. R. Koslowski, K. D. Lawson, M. Mantsinen, G. Matthews, F. Milani, M. Murakami, A. Murari, R. Neu, V. Parail, S. Podda, M. E. Puiatti, J. Rapp, E. Righi, F. Sartori, Y. Sarazin, A. Staebler, M. Stamp, G. Telesca, M. Valisa, B. Weyssow, K. D. Zastrow, and EFDA-JET Workprogramme Contributors, Nucl. Fusion **44**, 124 (2004).

[30]C. M. Roach, M. Walters, R. V. Budny, F. Imbeaux, T. W. Fredian, M. Greenwald, J. A. Stillerman, D. A. Alexander, J. Carlsson, J. R. Cary, F. Ryter, J. Stober, P. Gohil, C. Greenfield, M. Murakami, G. Bracco, B. Esposito, M. Romanelli, V. Parail, P. Stubberfield, I. Voitsekhovitch, C. Brickley, A. R. Field, Y. Sakamoto, T. Fujita, T. Fukuda, N. Hayashi, G. M. D. Hogeweij, A. Chudnovsky, N. A. Kinerva, C. E. Kessel, T. Aniel, G. T. Hoang, J. Ongena, E. J. Doyle, W. A. Houlberg, A. R. Polevoi, ITPA Confinement Database and Modelling Topical Group, and ITPA Transport

Physics Topical Group, "The 2008 Public Release of the International Multi-tokamak Confinement Profile Database," Nuclear Fusion (submitted).

[31] R. J. Hawryluk, in *Physics of Plasmas Close to Thermonuclear Conditions*, edited by B. Coppi, G. G. Leotta, D. Pfirsch, R. Pozzoli, and E. Sindoni (Pergamon, Oxford, 1981), Vol. 1, p. 19.

[32] J. Ongena, M. Evrard, and D. McCune, Trans. Fusion Technol. **33**, 181 (1998).

[33] R. V. Budny, D. R. Ernst, T.-S. Hahm, D. C. McCune, J. P. Christiansen, J. G. Cordey, C. G. Gowers, K. Guenther, N. Hawkes, O. N. Jarvis, P. M. Stubberfield, K.-D. Zastrow, L. D. Horton, G. Saibene, R. Sartor, K. Thomsen, and M. G. von Hellermann, Phys. Plasmas **7**, 5038 (2000).

[34] N. A. Uckan, *ITER Physics Design Guidelines*, ITER Doc. Series No. 10 (IAEA, Vienna, 1990).

[35] C. Bourdell, W. Dorland, X. Garbet, G. W. Hammett, M. Kotschenreuther, G. Rewoldt, and E. J. Synakowski, Phys. Plasmas **10**, 2881 (2003).

[36] G. W. Hammett, M. A. Beer, W. Dorland, S. C. Cowley, and S. A. Smith, Plasma Phys. Controlled Fusion **35**, 973 (1993).

[37] A. M. Dimits, T. J. Williams, J. A. Byers, and B. I. Cohen, Phys. Rev. Lett. **77**, 71 (1996).

[38] A. M. Dimits, G. Bateman, M. A. Beer, B. I. Cohen, W. Dorland, G. W. Hammett, C. Kim, J. E. Kinsey, M. Kotschenreuther, A. H. Kritz, L. L. Lao, J. Mandrekas, W. M. Nevins, S. E. Parker, A. J. Redd, D. E. Schumaker, R. Sydora, and J. Weiland, Phys. Plasmas **7**, 969 (2000).

[39] M. N. Rosenbluth and F. L. Hinton, Phys. Rev. Lett. **80**, 724 (1998).

[40] Y. Xiao and P. J. Catto, Phys. Plasmas **13**, 082307 (2006).

[41] E. A. Belli, Ph.D. thesis, Princeton University, 2006.

[42] Y. Xiao, P. J. Catto, and W. Dorland, Phys. Plasmas **14**, 055910 (2007).

[43] X. Q. Xu, R. H. Cohen, T. D. Rognlien, and J. R. Myra, Phys. Plasmas **7**, 1951 (2000).

[44] J. R. Ferron, M. S. Chu, G. L. Jackson, L. L. Lao, R. L. Miller, T. H. Osborne, P. B. Snyder, E. J. Strait, T. S. Taylor, A. D. Turnbull, A. M. Garofalo, M. A. Makowski, B. W. Rice, M. S. Chance, L. R. Baylor, M. Murakami, and M. R. Wade, Phys. Plasmas **7**, 1976 (2000).

[45] T. H. Osbourne, J. R. Ferron, R. J. Groebner, L. L. Lao, A. W. Leonard, M. A. Mahdavi, R. Maingi, R. L. Miller, A. D. Turnbull, M. Wade, and J. Watkins, Plasma Phys. Controlled Fusion **42**, A175 (2000).

[46] A. D. Turnbull, Y. R. Lin-Liu, R. L. Miller, T. S. Taylor, and T. N. Todd, Phys. Plasmas **6**, 1113 (1999).